Induced structural modifications in ZnS nanowires via physical state of catalyst: Highlights of 15R crystal phase

Sumit Kumar, Frédéric Fossard, Gaëlle Amiri, Jean-Michel Chauveau, Vincent Sallet

TABLE OF CONTENTS (TOC)

Induced structural modifications in ZnS nanowires via physical state of catalyst: highlights of 15R crystal phase

Sumit Kumar*[1], Frédéric Fossard[2], Gaëlle Amiri[1], Jean-Michel Chauveau[1], and Vincent Sallet*[1]

[1]Université Paris-Saclay, CNRS, UVSQ, France
[2]Université Paris-Saclay, CNRS, ONERA, France

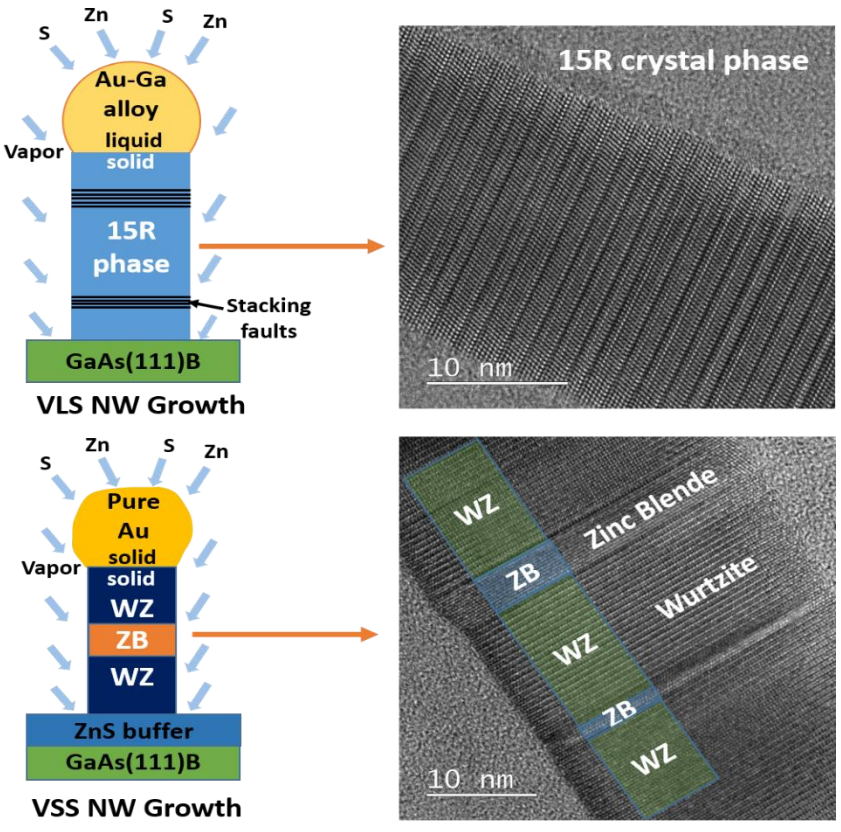

ZnS nanowires have been grown by two different approaches based on the physical state of the catalyst, specifically called VLS (vapor-liquid-solid) and VSS (vapor-solid-solid). Both approaches present unique structural properties, and remarkably, the crystallization of a 15R structure is highlighted in NWs grown by the VLS process.

Induced structural modifications in ZnS nanowires via physical state of catalyst: highlights of 15R crystal phase

Sumit Kumar[1] (✉), Frédéric Fossard[2], Gaëlle Amiri[1], Jean-Michel Chauveau[1] and Vincent Sallet[1] (✉)

[1] *Groupe d'Etude de la Matière Condensée (GEMAC), Université Paris-Saclay, CNRS - Université de Versailles St Quentin en Yvelines, 45 avenue des Etats-Unis, 78035 Versailles, France*

[2] *Laboratoire d'Étude des Microstructures (LEM), CNRS-ONERA, Université Paris-Saclay, 29 avenue Division Leclerc, 92322 Chatillon, France*

KEYWORDS

II-VI semiconductors, MOCVD, vapor-liquid-solid (VLS), vapor-solid-solid (VSS), TEM analysis, polytypism

ABSTRACT

Peculiar and unique growth mechanisms involved in semiconductor nanowires (NWs) pave the way to the achievement of new crystallographic phases and remarkable material properties, and hence, studying polytypism in semiconductor NWs arouses a strong interest for the next generation of electronic and photonic applications. In this context, the growth of ZnS nanowires has been investigated, as bulk ZnS compound exhibits numerous unstable polytypes at high temperatures, but their stable occurrence is highly anticipated in a nanowire due to its special quasi-dimensional shape and growth modes. In this work, the idea is to provide a change in the growth mechanism *via* the physical state of catalyst droplet (liquid or solid) and study the induced structural modifications in ZnS nanowires. The HRTEM images of VLS (*via* liquid alloyed catalyst) grown ZnS NWs show periodic stacking faults, which is precisely identified as a stacking sequence of cubic or hexagonal planes leading to an astonishing 15R crystal polymorph. This crystallographic phase is observed for the first time in nanowires. Contrastingly, NWs grown with VSS (*via* solid catalyst) show crystal polytypes of zinc blende (3C) and wurtzite (2H). We calculated and discussed the role of cohesive energies in the formation of such ZnS polytypes. Further, we presented the selection rules for the crystallization of such 15R structure in NWs and discussed the involved VLS and VSS growth mechanisms leading to the formation of different crystal phases.

1 Introduction

II-VI semiconductor nanowires (NWs) have been extensively studied because of their potential applications in nanowire-based electronics, future generation electronics and optoelectronic nanodevices [1, 2]. The quasi-one-dimensional (1D) shape of nanowires and a large surface-to-volume ratio enable tailoring the material properties and photonic applications [3]. For instance, a quantum dot embedded in a NW allows the confinement of carriers (electrons and holes) which can be used as a photon emitter for quantum optics [4]. In addition, nanowires exhibit peculiar crystal phases that may differ from their thin film and bulk counterparts, and attract researchers to study their fundamental science [5, 6]. Indeed, III-V, II-VI and elemental semiconductor NWs adopt remarkably the wurtzite (WZ) structure in contrast to their bulk form, except for GaN and ZnO for which the wurtzite bulk structure is kept.

In materials science, polytypism (or polytypes) is a special case of polymorphism where different polymorphs exist in different domains within a crystal. In the past, it has been extensively studied in bulk materials at high temperatures specially for SiC and ZnS compounds [7-9]. Interestingly, in the case of 1D nanostructures, polytypism can arise due to the particular growth mode below a catalyst droplet, that may induce different stacking sequences along the length of the nanowire. In semiconducting NWs, a high density of randomly distributed twin defects and stacking faults has commonly been observed [10, 11], as well as random mixtures of cubic and hexagonal phases [12]. However, the stacking faults can be correlated [13] and form ordered arrays, until giving rise to new phases (polytypes) with distinct properties [14]. Hence, 4H, 6H, 8H, and 10H (so-called high order polytypes) have been observed in Ge, Si, GaAs, InAs and ZnS nanowires [15-18]. As regards the fabrication method, the vapor-liquid-solid (VLS) approach [19] using the liquid catalyst droplets has usually been exploited to grow semiconductor nanowires. In VLS growth, the different crystal structures have been correlated with the shape and contact angle between the droplet and nanowire interface that changes the capillary forces at triple phase line (TPL) [5]. Dubrovskii *et al*. [20] as well as Glas *et al*. [21] have thoroughly investigated the nanowire growth and have proposed theoretical models to describe the involved mechanisms, taking into account the diffusion of atoms, nucleation site, relevant surface energies and supersaturation in the catalyst droplet. All these parameters play a significant role to determine the crystal structure and the occurrence of polytypes.

In this article, we were interested to achieve new crystallographic phase in ZnS nanowires. ZnS was one of the first discovered compound semiconductor and has been widely used in flat panel displays, UV sensors, electroluminescent devices, infrared windows [22, 23]. ZnS nanostructures offers fascinating properties such as direct wide bandgap (3.72 eV for cubic zinc blende (ZB, being the most stable crystal phase) and 3.77 eV for hexagonal wurtzite (WZ)), presence of polar surfaces, high electronic mobility, and thermal stabilities [24]. Most importantly for this study, ZnS offers a very wide range of possible polymorphs, all currently identified and listed in reference [7], with a number of layers in the elementary stacking sequence up to 64. Similar to SiC, the common 4H, 6H, 8H and 10H phases were observed in ZnS, as well as the 15R phase [25]. Noticeably, if the structural properties of such polytypes, *i.e.* the identification of the stacking sequences, have been experimentally characterized and even theoretically explained in the framework of the Axial Next-Nearest-Neighbor Ising (ANNNI) model, their optical properties remain almost unknown (except for the cubic and hexagonal phase). Boutaiba *et al.* [26] have calculated the band structures of 2H, 4H, 6H, and 3C phases, all predicting a direct bandgap, with an energy varying from 3.8 (for pure cubic) to 3.88 eV (pure hexagonal). Regarding the 15R phase of ZnS, a change in the band structure is also expected, analogously to the case of 15R ZnO [27].

The objectives of this work were threefold:

i) carry out an experimental study to grow vertical arrays of ZnS NWs with controlled morphology,

Address correspondence to Sumit Kumar, sumit.kumar@uvsq.fr; Vincent Sallet, Vincent.sallet@uvsq.fr

crystal structure, and defects. Indeed, we predict twins and stacking faults to easily occur due to a low formation energy. For comparison, the experimental intrinsic stacking fault energy in zinc blende (E_{ISF}) is less than 6 mJ/m², and 45 mJ/m² in GaAs [28].

ii) identify possible new phases, appearing upon specific growth conditions. In the light of the variety of ZnS polytypes available in the bulk form [7], the occurrence of different crystal structures is highly expected in ZnS NWs with tuning the growth parameters. As the electronic structure varies with crystal structure, the achievement of new phases in semiconductors would pave the way to novel physics and original applications. For example, a new h-Si6 silicon phase with direct bandgap was reported to be an efficient solar absorber [29]. In SiC, well-known material for its polytypism, a quantum crystal phase heterostructure (but homomaterial) was fabricated by embedding a 3C well in 4H barriers [30]. Indeed, similarly to the case of III-V NWs [31, 32], we expect that new ZnS polymorphs would be useful for designing crystal phase heterostructures, bandgap engineering, enhanced thermal and mechanical properties, and direct intersubband optical transitions. Controlling the crystal structure (*e.g.* by adjusting the supersaturation during the nanowire growth) would enable the design of original hetero-crystalline (but single ZnS) junctions, without compound intermixing at the interfaces, thus having potential applications in the UV emission.

iii) introduce vapor-solid-solid (VSS) growth. A drawback of the VLS process is that atoms from the liquid droplet can be incorporated as impurities during the NWs growth resulting in the degradation of the optical properties. Moreover, in order to produce heterostructures with perfectly abrupt interfaces, a major problem to face is the reservoir effect (or memory effect) due to the liquid droplet, when switching the NW growth from material A to material B. These issues can be tackled by using a solid catalyst and growing the NW in the so-called vapor-solid-solid (VSS) mode [33], the solubility of a given substance in a solid being much lower than that in a liquid.

To date, ZnS NWs have been synthesized by various techniques but most of these techniques result in randomly aligned nanoribbons or nanotubes growth [34, 35]. Herein, the vertical arrays of Au-assisted ZnS NWs on GaAs (111)B by metalorganic chemical vapor deposition (MOCVD) following either the VLS or the VSS process have been achieved. To the best of our knowledge, this is the first study reporting on the Au-assisted VSS (*via* solid catalyst) grown ZnS nanowire. In order to force the Au-droplet to remain solid, we inserted a ZnS buffer on the GaAs (111)B substrate and consequently modified the catalyzed mechanism. On providing a change in the growth mechanism *via* the physical state of catalyst droplet (liquid or solid), we were able to tune the morphology and crystal structure of the ZnS nanowires. A comparison of the VLS and VSS growth mechanisms is detailed on the basis of NWs morphology, crystal quality and structural evolution assessed by scanning and transmission electron microscopies, and energy dispersive x-ray spectroscopy (EDS). It is reported that ZnS NWs grown directly on GaAs exhibit 15R crystallographic structure and alloyed Au-Ga droplet on their top (inducing a VLS process), whereas NWs grown on ZnS(buffer)/GaAs show stacking of WZ and ZB domains, with pure Au droplet, which confirms a VSS mechanism. Further, cohesive energy calculations are given to better understand the occurrence of stacking defects and high order polytypes in ZnS. The involved growth mechanisms are discussed on the basis of the knowledge related to III-V and II-VI NWs.

2 Experimental

Au-assisted ZnS NWs were grown on GaAs (111)B and ZnS (buffer)/GaAs (111)B in a vertical MOCVD reactor operating at atmospheric pressure. The catalyzed fabrication process is illustrated in Figure 1. The susceptor was heated up using a RF generator and the reactor walls were cooled to 20 °C in order to limit the parasitic depositions. Diethylzinc (DEZn) and ditertiarybutylsulfide (DTBS) were used as the zinc

and sulfur precursors respectively. Hydrogen was used as carrier gas. In the case of samples with ZnS buffer, GaAs substrates were deoxidized at 550 °C followed by the deposition of a 900 nm thick ZnS layer.

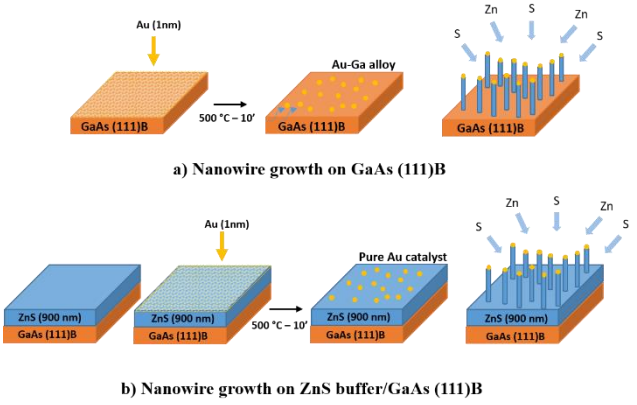

Figure 1. The schematic diagram of ZnS NWs growth on a) GaAs (111)B, b) ZnS (buffer)/GaAs (111)B, where a thick buffer layer was prepared to prevent the gold particles from interacting with the substrate.

Prior to NW growth, a 1 nm thick Au layer was deposited at room temperature on the substrate surface using thermal evaporation. The samples were then transferred into the MOCVD reactor where 10 minutes annealing at 500°C under H_2 was performed to ensure Au de-wetting. Afterwards the temperature was fixed to 550°C for the growth of ZnS NWs for 3 min. The DEZn and DTBS precursor partial pressures were 8 Pa and 16 Pa for zinc and sulfur, respectively, giving a VI/II ratio of 2. These partial pressures correspond to a S-rich growth regime. The optimization of growth parameters to achieve vertical NWs is out of scope of the present article and will be published elsewhere. After growth, the morphology of the NWs was examined using Scanning Electron Microscopy (SEM, JEOL 7001F). We have observed that the long insulating wires undergo charge accumulation by the electron beam, causing the bending of the nanowire while the beam was scanning. Thus, the accelerating voltage must be decreased at 10-15 kV to eliminate this effect. Transmission Electron Microscopy (TEM) was used to determine the crystalline structure of the NWs, including the catalyst nanoparticle on their top. NWs were removed from their substrates by scratching the surface and spreading on a TEM copper grid covered with a holey carbon film. The grid was inserted in a Zeiss Libra 200 MC TEM equipped with a monochromator and an in-column filter. The microscope was operated at 200 kV to achieve a lattice resolution below 1.5 Å in High Resolution mode. High Angle Annular Dark Field (HAADF) images and Energy Dispersion Spectroscopy (EDS) were performed in Scanning TEM mode with a nanometric probe.

3 Results

3.1 Nanowire Growth

In this study, we aimed to focus on the influence of a ZnS buffer layer on which Au droplets would lay. To do so, both substrates with and without buffer were kept in the same run, in order to grow the ZnS NWs in the same conditions. The SEM images of the samples are shown in Figure 2 (cross-sectional view of the NWs are shown in Figure S1, Elect. Suppl. Material, ESM). Straight and vertically oriented NWs were observed in both cases. NWs grown on GaAs (111)B substrate has length in the range 350 – 1400 nm with diameter 10 – 35 nm below the droplet. Contrastingly, thinner and shorter NWs were observed on ZnS buffer samples, with length 230 – 590 nm and diameter ranging 7 – 25 nm, as well as worm-like and kinked NWs with larger diameter around 25-30 nm. The variation in diameter can be correlated to the catalyst size at the top of nanowire. In addition, on careful analysis of the Figure 2a and 2b, it can be seen that the droplet at the top of nanowire grown on GaAs (111)B is larger in size compared to the one of the nanowire with buffer. This behavior suggests that only small catalysts are assisting the nanowire growth in case of "with buffer" growth [36]. In 2014, Zannier *et al*. have similarly observed a diameter dependent morphology of VSS grown ZnSe NWs [37]. Their NWs with diameter below 15 nm were straight while thicker nanowires showed a "worm like" morphology distinguished by multiple kinks. This support the idea that there exists a critical diameter of the catalyst above which growth of straight nanowires is suppressed by either development of kinks or formation of a 2D layer on catalyst. In our samples, straight and kinked NWs can be seen more clearly in TEM images (Figure 4a).

We measured a maximum growth rate of 7.7 nm/sec in the case of ZnS NWs grown on GaAs (111)B, and 3.3 nm/sec for NWs on buffer samples. In MOCVD process, this agrees with a preferential adsorption of DEZn and DTBS precursors on the liquid droplet rather than on the solid, or as a higher solubility of one or both of the reactants in the liquid, which leads to an increase of the reactant flows at the TPL. Such discrepancy of the growth rate between the two processes was also observed in Ge NWs growth [38].

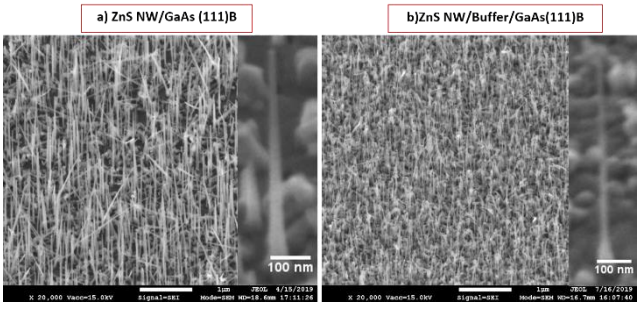

Figure 2. 45° tilted SEM images of NWs grown on a) GaAs (111)B, array of vertical ZnS nanowires with catalyst droplet at the top, and b) ZnS buffer/GaAs (111)B, array of thin and vertical ZnS nanowires.

3.2 Structural analysis

In following section, we compare the structural properties of the two types of NWs, grown with or without ZnS buffer. The STEM/HAADF image of a single nanowire grown on GaAs (111)B is shown in Figure 3a. The gold catalyst is clearly seen at the top. The diameter below the droplet is 19 nm, and increases to 30 nm at the bottom, suggesting a relatively small contribution of the lateral growth on the NW sides during the process. An HRTEM image taken in the [010] zone axis is given in Figure 3c, and it shows periodic material stacking along the growth direction, which could correspond to WZ-ZB modulations and/or stacking faults. The thickness of each modulation (as it appears in the image) is around 2 nm. Similar kinds of structural patterned HRTEM images have been observed in the past, showing mixed zinc blende and wurtzite phases and appearance of stacking faults [11, 17, 39-42]. In particular, Liang *et al*. reported the vertically oriented growth of ZnS NWs assisted by Au, Ag and Ga catalysts [39, 43] and emphasized the crystal phase dependence upon NW diameter. In their ZnS NWs, Jiang *et al*. also described a modulation of structure at the nanometer scale as a stacking of 8H and 10H half-cells [17]. Herein, we seized the opportunity to perform profound investigation on the structural pattern observed in HRTEM image. An accurate analysis of the ordered stacking sequence reveals the formation of a complex structure in a periodical manner along the length of NW. The repeated sequence corresponds to ABCBA-CABAC-BCACB planes, and consists of 3 cycles (each one containing 5 planes with a mirror sequence, *e.g.* AB$\underline{C}$BA) with circular permutations. Such crystal structure is known as 15R [44]. The 15R polymorph crystallizes in the rhombohedral (or trigonal) system, with the space group being R3m. The crystal structure fits well on superimposing a 15R model on the Fourier filtered image of nanowire as shown in Figure 3d. This polymorph is highlighted for the first time in ZnS NWs while it is usually observed for SiC [9, 45]. The phase transition of ZnS minerals was reported by Akizuki in 1981 and similar stacking pattern of 15R structure was observed by HRTEM [25]. In 1948, Frondel and Palache experimentally observed the three polymorphs (4H, 6H and 15R) in ZnS system and calculated the cell parameters [46]. In Figure 3b, the FFT pattern signifies a 5-fold symmetry and confirms the presence of (0015), (107), and (10$\bar{8}$) planes in close agreement with such 15R cell parameters. Conventional TEM images (bright field and dark field) and diffractions have been performed on several tens of nanowires (see ESM, section S-1). The signature of the 15R phase given in diffraction by the peculiar pattern (*i.e.* a 5th order superstructure) has been observed in all investigated wires, with a diameter dispersion from 15 to 40 nm. We have no evidence that a critical diameter prevents or inhibits the 15R growth with respect to this investigated range of nanowire diameters. In addition, dark field images show that the polytype formation is not continuous all along the nanowire, however 15R segments with lengths of a few tens of nanometers are frequently revealed.

In comparison, the TEM image of a single nanowire grown on ZnS/GaAs (111)B (*i.e.* with buffer)

is shown in Figure 4a. Contrastingly to the previous sample, in this case the gold catalyst is believed to remain solid, since the ZnS buffer impedes the diffusion of Ga from the substrate. The straight and worm-like kinked NWs are distinguished with blue and yellow markers respectively. Interestingly, the stacking sequence of HRTEM image discloses separate and large domains (Figure 4b). The FFT pattern given in Figure 4c and 4d indicate the formation of pure WZ and ZB domains, respectively.

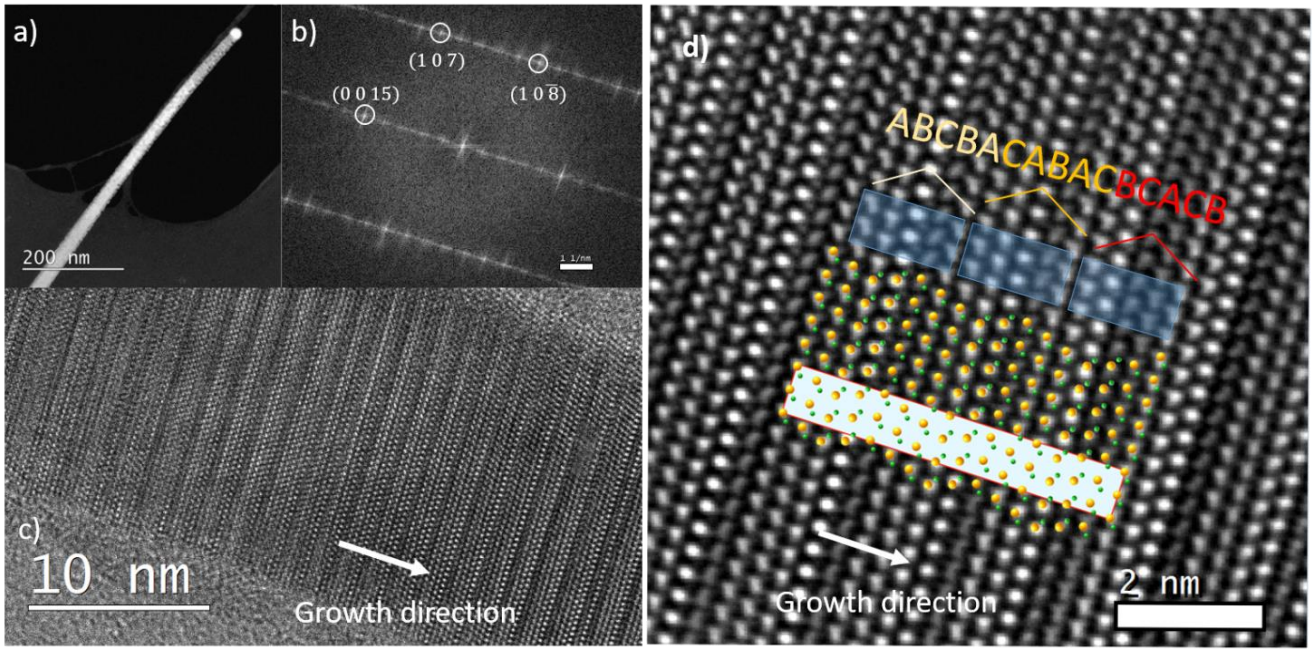

Figure 3. a) STEM/HAADF image of a single nanowire grown on GaAs (111)B, b) Fast Fourier Transform (FFT) pattern, c) HRTEM image of nanowire, d) Fourier filtered image superposed with 15R structure model and the respective stacking sequence ABCBA-CABAC-BCACB.

More in details, the NW contains large segments of WZ with inclusion of short 1 – 15 nm thick ZB phases (with average of 4 nm). The stacking sequence at the interface of WZ and ZB is confirmed to be ABABABCABC. With the help of FFT pattern, we find that the NW grew in the [0001] and [111] direction for WZ and ZB phases, respectively, which is commonly observed in semiconductor NW growth. Moreover, we have not found any visible correlation between the diameter of NW and length of WZ or ZB phases (refer Figure S2, ESM).

The HRTEM analysis also focused on the catalyst droplet at the top of nanowire to validate the VLS and VSS credibility (refer section S-2, ESM). In VLS case, the FFT pattern of HRTEM image corresponds to the Au7Ga2 phase of the catalyst at room temperature. Whereas, the catalyst shows a facetted shape and the corresponding FFT pattern confirms the pure gold phase of the catalyst with a face-centered cubic structure.

In addition, EDS analysis of the catalyst droplet present at the top of the nanowire was performed (refer section S-3, ESM). Regarding NWs grown directly on GaAs (111)B, Ga and Au contents were detected, but no presence of Zn or S (or below the detection limit) has been found. On the other hand, EDS analysis of the tip of a nanowire grown with ZnS buffer only shows the presence of gold with no detectable traces of gallium, Zn, or S. Both HRTEM and EDS analysis validates the VLS and VSS growth processes for the NWs grown on GaAs (111)B and ZnS buffer/GaAs(111)B respectively.

To summarize the experimental part, when ZnS NWs were grown on GaAs (111)B substrates assisted by Au (*i.e.* VLS growth), we observed an interaction between the catalyst and the substrate, leading to the formation of Au – Ga alloyed droplet, which is liquid at growth temperature. Considering the fact that the physical state of catalyst might affect the structural properties of ZnS NWs, we prepared a thick ZnS

buffer layer on GaAs (111)B to cease the interaction of Au gold catalyst with the substrate. Hence, in this case, we observed that the NWs growth were assisted by the pure solid Au catalyst (*i.e.* VSS growth) at 550 °C (melting point of Au is 1064 °C). However, one can argue that the physical state of catalyst may also depend on the binary systems Au-Zn and Au-S, and this will be discussed later in the VSS section.

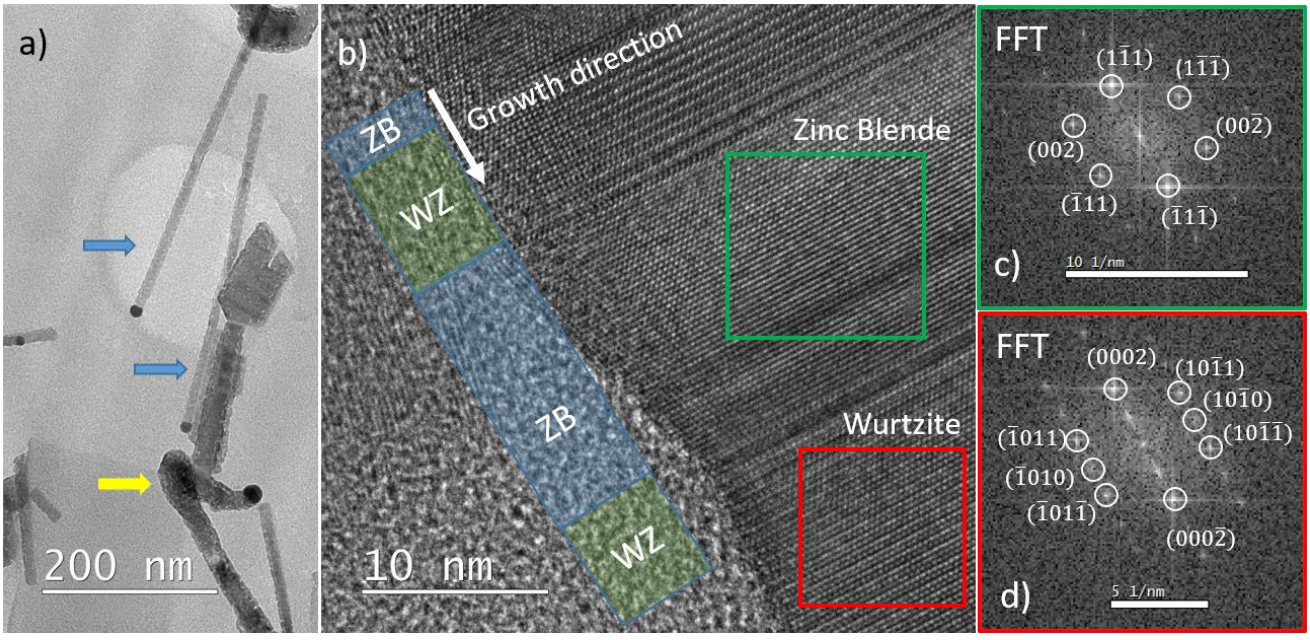

Figure 4. a) TEM image of a single nanowire grown on ZnS buffer/GaAs (111)B, b) HRTEM image with single domains of ZB and WZ phase, c) FFT pattern of a ZB segment, d) FFT pattern of a WZ segment.

4 Discussion

4.1 Occurrence of polytypes in ZnS

We use to consider that a plane is wurtzite (and noted h) if sandwiched between a previous plane and a next plane having the same lateral position (*e.g.* A<u>B</u>A), and zinc blende (noted c) if different positions (*e.g.* A<u>B</u>C) [47]. Another method could better take into account the fact that we are growing material. Considering the crystal projection in the [010] zone axis, if the Zn-S bonds (not normal to the growing plane) of the newly deposited ML are parallel to the corresponding bonds of the previous ML, then the new ML is 'c', and if not, the new ML is 'h' (refer Figure 6a). The small difference in cohesive energy between ZB and WZ structures (*i.e.* 7.8 mJ/m^2) enables the occurrence of twins and stacking faults in ZB ZnS. Consequently, the formation of stacking faults in a periodic manner qualitatively can result in the formation of high order polytypes. The cohesive energy calculations of the polytypes in ZnS can give us an idea about their occurrence possibilities. Simple calculations have been earlier proposed by Glas [47] considering

$$\partial E_p = \frac{N_h \partial_1 - 2n\partial_2}{N_h + N_c} \qquad (1)$$

interactions up to the second neighbor monolayer (ML). The expression of the cohesive energies for different ZnS polytypes considering the lattice spacing of 0.31 nm (d_{111} for ZB or d_{0001} for WZ) is written as,

Here δ_1 is the cohesive energy difference between the cubic and hexagonal layer per unit area of ML, δ_2 is the

$$\text{Hexgonality}\ (\%) = \frac{N_h}{N_h + N_c} \times 100 \qquad (2)$$

increase in energy as a result of stacking faults, N_h and N_c are number of hexagonal and cubic layers, and n is the number of nonempty sequences of cubic planes. The hexagonality of a polytype is defined as the ratio of the number of hexagonal layers to the total number of layers in the crystal and can be expressed as,

Using δ_1 = 7.8 mJ/m² and δ_2 = 4.8 mJ/m² [47], the cohesive energies of ZnS polytypes are calculated and plotted as a function of their hexagonality. Results are gathered in Table 1 and Figure 5.

Indeed, all cohesive values are very close for different polytypes. Here, the negative energy would simply mean a more stable structure for a given stack compared with 3C (ZB), so that 6H, 15R and 4H structures could be the most stable polytypes of ZnS. The conclusion that all phases from 3C (pure cubic) to 4H are expected to easily occur, and 2H (pure Hexagonal) is the less favorable (but again with a small increase of the cohesive energy), agrees with previously published calculations [8, 26, 48].

Polytype	**Stacking sequence**	**Hexag-onality (%)**	**Formula**	∂E_p(mJ/m²)
3C	ABC	0	0	0
8L	ABACBACB	25	$\frac{1}{4}\partial_1-\frac{1}{4}\partial_2$	0.75
6H	ABCACB	33	$\frac{1}{3}\partial_1-\frac{2}{3}\partial_2$	-0.6
15R	ABCBACABA CBCACB	40	$\frac{2}{5}\partial_1-\frac{4}{5}\partial_2$	-0.72
4H	ABCB	50	$\frac{1}{2}\partial_1-\partial_2$	-0.9
9R	ABACACBCB	67	$\frac{2}{3}\partial_1-\frac{2}{3}\partial_2$	2
2H	AB	100	∂_1	7.8

Table 1. The table includes the cohesive energy expressions and their calculated values for different ZnS polytypes with their respective hexagonality.

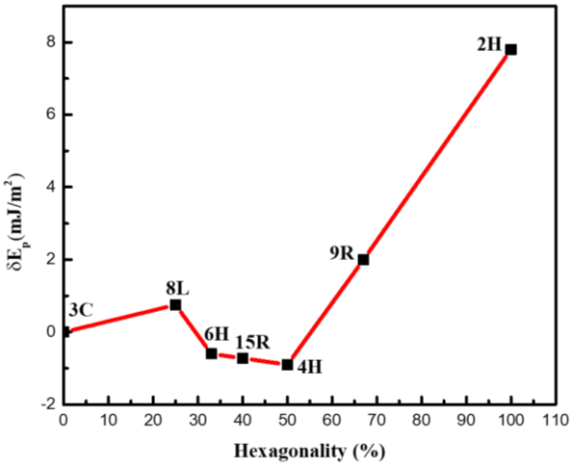

Figure 5. The plot of cohesive energies of ZnS polytypes (with respect to 3C (ZB) structure) as a function of their hexagonality (in percentage) shows that 6H, 15R and 4H having the minimum cohesive energies are most stable.

4.2 15R polytype in VLS growth

It is remarkable that VLS and VSS processes lead to different crystal structures of the grown ZnS NWs. In particular, TEM analysis revealed a 15R phase in the VLS grown NWs. If we look into the detail at the stacking sequence ABCBA-CABAC-BCACB illustrated in the Figure 3d, the 15R structure exhibits cubic and hexagonal planes in a periodical manner, and stacked along the growth direction, <111> for zinc blende, ABCABC…, and <0001> for wurtzite ABAB.... Relative to ABCBA-CABAC-BCACB repeated cell, that gives a hcchc-hcchc-hcchc stacking sequence as shown in Figure 6. The 15R crystal structure is referred as 32, a sequence of 3 planes and a sequence of 2 planes repeated three times to give a stacking of 15 planes (refer Figure 6c) in Zhdanov notation [49]. The first sequence of 3 planes have Zn-S bonds in one direction, and the following 2 planes have corresponding bonds in the other direction, so that the structure can be seen as a ZB zig-zag structure. It can also be described as the stacking of 3 untwinned ZnS tetrahedra followed by 2 twinned tetrahedral [9]. Therefore, we can introduce the notation A', B' and C' to take into account such rotation of the bonds around the vertical direction, as illustrated in figure 6a. The 15R structure observed in our ZnS NWs is now fully described as ABCB'A'-CABA'C'-BCAC'B'. In the 3 cycles of 5 planes, the periodic rotation of the first

plane is noteworthy. Each cycle shows a "mirror" plane, namely the third one at the center, which can be considered as a twin, *e.g.* plane C in the ABCB'A' cycle.

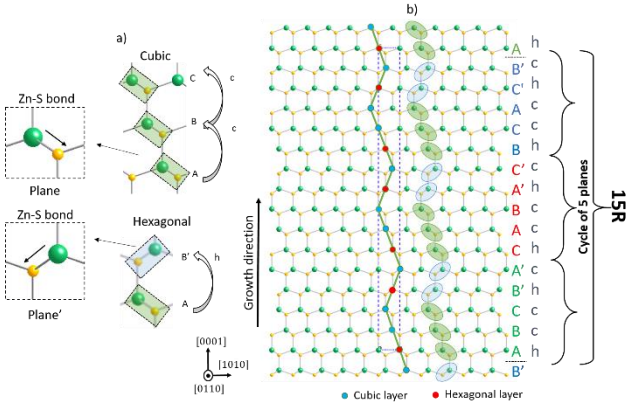

Figure 6. a) Notation of the planes (plane and plane') with respect to the direction of bonds, and the stacking of hexagonal (h) and cubic (c) planes, b) the structural model of 15R structure with 3 cycles of 5 planes, giving the ABCB'A'-CABA'C'-BCAC'B' sequence.

The conditions needed to crystallize the 15R structure could be analyzed by examining the hcchc-hcchc-hcchc stacking. We introduce two descriptions which can be seen as a growth mechanism with certain rules.

Description 1: growth mechanism considering monolayer by monolayer deposition. The 15R crystal structure can be built with the four following rules: i) h → c, ii) cc → h, iii) cchc → h and iv) hchc → c, where we put the underlying MLs at the left of the arrow and the new ML at the right. There is no hh stacking, letting assume that the hexagonal phase formation is unfavorable, in agreement with cohesive energies calculations. We thus mark that there is a strong tendency to alternate c and h MLs, with only one exception of the 4th transition (*i.e.* c plane is deposited on c). This exception makes all the difference between crystallization of 15R with that of 4H (chchch stacking). It implies that, during the growth of a new ML, the interaction can involve up to 4 underlying MLs. Such interaction beyond the nearest neighboring ML has been reported by Johansson [50] and Priante [13] in III-V NWs growth and investigated in the framework of ANNNI model (Axial Next-Nearest-Neighbor Ising model).

Description 2: growth mechanism considering the stacking fault formation. The sequence 'hch' in ZB (cubic) structure is labeled as an extrinsic stacking fault (ESF) [47]. On considering the ESF, the crystallization of 15R can be predicted with only 1 rule: cc → hch (ESF) →cc. It means after every cc (cubic) sequence, the crystallization of a stacking fault is occurring. The energetic calculations for different stacking faults (intrinsic stacking fault (ISF), twin stacking fault (TSF) and ESF) in ZB ZnS will provide a clear sight on the type of stacking fault to be favored. We calculated these energies values using the same parameters as presented in equation (1) [47].

$$E_{\mathrm{ISF}}^{\mathrm{ZB}} = 2(\partial_1 - \partial_2) = 6\ \mathrm{mJ/m^2}$$
$$E_{\mathrm{twin}}^{\mathrm{ZB}} = \partial_1 - 2\partial_2 = -1.8\ \mathrm{mJ/m^2}$$
$$E_{\mathrm{ESF}}^{\mathrm{ZB}} = 2(\partial_1 - 2\partial_2) = -3.6\ \mathrm{mJ/m^2}$$

Therefore, ESF having the minimum energy will be more likely to occur. It has to be nevertheless noted that having the minimum energy is not the unique condition to favor ESF in ZB, since such occurrence is also dependent on growth conditions as well as on surface and edge energies [6, 51].

As previously mentioned, twins boundaries, stacking faults and polytypes are commonly observed in semiconductor NWs growth [52-54]. A nucleation-based model has been proposed by Glas *et al.* [6] and Dubrovskii *et al.* [55] to explain crystal phase switching between ZB and WZ during the catalyzed growth of NWs. In this model, nucleation at the triple phase line (TPL, at the edge of the solid-liquid interface, thus in contact with the vapor) favors the formation of the WZ structure, while nucleation away from the TPL (within the nanowire-liquid interface), leads to ZB growth. Thus, identification of the exact nucleation site is key to understanding the mechanisms of phase selection in NW growth. Experimentally, performing *in situ* GaAs NW growth in a TEM, it has been shown that the crystal phase of the NW is governed by the contact angle of the catalyst droplet [5]. Droplet geometry could be varied with the group III and group V fluxes. A critical contact angle around 125° has been measured which defines a transition between WZ growth at the TPL (<125° [51],) and ZB growth (>125°, with edge truncation [5, 56]).

Interestingly for II-VI compounds, and without carrying out *in situ* observations, Hao *et al.* [11] had early reported periodic twins in a ZB ZnS NWs and had presented a growth model where the droplet geometry would vary during the growth. They explained that when growth conditions (mainly high growth temperature) lead to the situation that the diffusion of species in the liquid catalyst is slower than crystal growth at the L-S interface, periodic depletion of Zn and S results in a modulation of the droplet contact angle, due to a change in the wettability.

In our experiments, similarly to III-V NWs, the change in the nucleation site could be related to the modulation of the droplet contact angle. We measured a contact angle between 110 and 123°, close to the critical angle reported for GaAs (125°). Without stating that ZnS and GaAs VLS cases are equal, this may aid the discussion about the involved mechanism. A small variation of the contact angle around its critical value would bring a ZB (c) or WZ (h) plane formation. At the moment, the origin of this particular hcchc-hcchc-hcchc stacking is still to be precised, but the door is now open for a theoretical study, primarily in the light of the ANNNI model. On the basis of such knowledge, and considering the surface energies, edge energies and the preference for the nucleation site in ZnS NWs, it might be possible, in a future work, to model the nucleation mechanism involved in formation of the 15R phase or other polymorphs. As regards growth parameters having a strong influence on the crystal structure, precursor partial pressures (which controls the supersaturation) are believed to play a major role [57]. For example, we expect growing VLS ZnS nanowires with low partial pressures (low supersaturation, but same VI/II ratio) would give 3C cubic phase like in the GaAs case.

4.3 The case of solid catalyst (VSS)

VSS growth involving solid Au-catalyst has been reported for many semiconductors such as GaAs, InAs, Si, Ge, ZnSe, ZnTe, ZnO [33, 37, 58-61]. In this process, atoms from the vapor phase adsorbing on the Au particle would diffuse in the body towards the growing interface. However, it is still not clear whether the reactants are actually incorporated into the catalyst or would diffuse on the surface to reach the interface edge (similar to the TPL in VLS, in the following section referred as "pseudo-TPL"), and further crystalize at the S-S interface. Like in VLS, diffusing adatoms from the substrate and from the NW sidewalls could also contribute to the growth. In our case, we assume that there is no incorporation of S in the Au-droplet at 550°C due to high volatilization of sulfur [62]. The Au_2S alloy may exist, and has been synthesized and investigated by Ishikawa *et al.* [63] but it was shown to decompose at temperatures above ~500K. It is difficult to state if Zn diffuses in the droplet. At 550°C, considering the phase diagram, the Au-Zn alloy can be in the liquid state but only for high Zn contents, in the range [85-100%] [64]. Such strong diffusion of Zn in the Au-particle is not expected. In the literature, there is neither evidence of liquid Au-Zn alloy catalyzing the NW growth, *e.g.* in the case of ZnTe or ZnSe at temperatures between 350° and 450°C. Interestingly, at much higher temperature (900°C), Simon *et al.* [61] proposed a growth model involving an Au-Zn (8.5-12.5% Zn) liquid skin at the surface of the catalyst to describe the growth of ZnO NWs, where zinc atoms diffuse towards the pseudo-TPL and react with oxygen atoms. In our grown ZnS samples, EDS analysis of the catalyst show no detectable Zn, nor S, letting impede that the droplet remains solid, leading to a VSS growth. Reactant species are believed to be mainly transported *via* diffusing through the solid Au surface, as well as along the NW sidewalls [65, 66]. However, a contribution of a small fraction of Zn or S diffused in the solid cannot be fully rejected, as we know that, for example, GaAs NWs are grown using an As content in the Au-Ga catalyst as low as 0.01% [67].

In contrast with VLS, ZnS NWs grown with solid catalysts exhibit pure WZ and ZB domains and alternates between these two structures. Due the solid state of the Au-particle, the diffusion of Zn and S atoms at the solid-solid interface is reduced and their transport towards the inner part of the growth front is slow [37]. Consequently, a new growing plane could start to nucleate before the last one has completed [61]. This may lead to instabilities affecting the growth front geometry, which could be either flat,

symmetrically facetted, or asymmetrically facetted (see figure 7), as well as impacting surface energies of the new interface and the contact angle at the pseudo-TPL. Then, nucleation can occur at different sites leading to stacking defects, kinks and crystalline phase changes. In particular, it has been suggested that slow growth kinetics in VSS process produce the worm-like nanowires [37, 68, 69]. Similar to the case of ZnSe NW growth [37], we observed that small catalyst particles (10-20 nm in diameter) lead to a flat droplet-NW interface and a straight wires, whereas worm-like and kinked nanostructures are induced by large and facetted Au-droplets. Rueda *et al.* [60] also demonstrated that the crystal structure of VSS grown ZnTe nanowires is gold particle geometry dependent. A half sphere catalyst (*i.e.* small contact angle) matching the diameter of the NW resulting in a WZ crystal phase, whereas a full sphere gold catalyst particle (*i.e.* large contact angle) was found at the tip of ZB NW.

At the difference of VLS process involving a liquid droplet, high order polytypes are not observed when the catalyst remains solid. This could be understood by the modified growth kinetics, as well as the surface energy difference between pure Au and Ga-Au surface [70]. Also, the 15R could occur in a particular range of supersaturation in VLS, as proposed in the work of Johansson *et al.* [71], where the density of staking faults and WZ segments in ZB GaP NWs is related to the concentration of reactants in the catalyst. In addition, the liquid or solid state of the catalyst may involve distinct growth processes at the droplet/NW interface: ML by ML growth observed as *in situ* grown GaAs can be assumed for VLS NWs, in contrast with multiple nucleation at the solid-solid interface in VSS.

Another feature is that VSS involves segments of pure hexagonal phase in the NW. This particular growth condition overcomes the limitation of 2H occurrence due to a higher cohesive energy. This confirms that the occurrence of a particular phase in semiconductor NW growth is not only dependent on the cohesive energy but also on thermodynamics and growth conditions. That promotes the high potential and the great interest of nanowire growth studies, and make the field promising to achieve new and unexpected crystallographic phase in semiconductors.

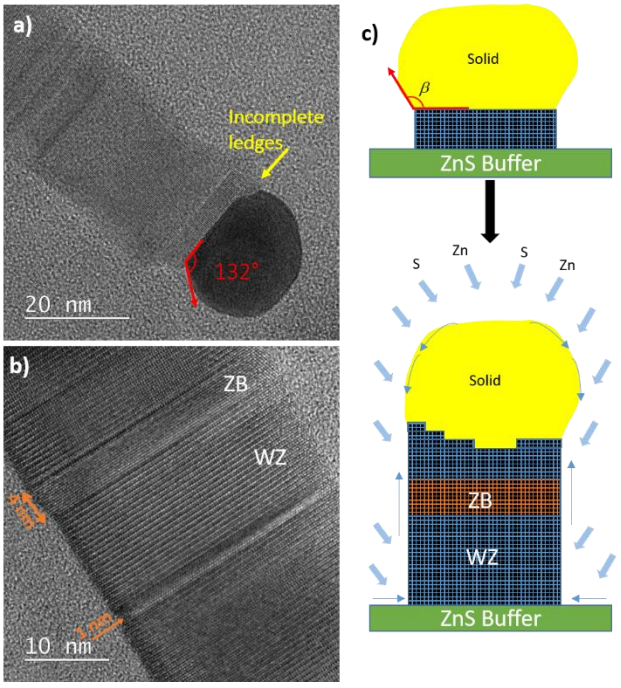

Figure 7. a) The faceted droplet with incomplete ledges (or layers), b) the stacking of small ZB segments (1 and 4 nm) in the WZ structure, c) the model showing formation of ledges (incomplete layers) with a faceted solid droplet at the top.

5 Conclusions

In conclusion, we have demonstrated that different crystallographic phases in ZnS nanowires could be achieved by varying the NW growth mechanisms. Two different Au-catalyzed growth approaches, namely VLS and VSS, were employed to grow vertically aligned ZnS NWs by MOCVD. In the VLS case, the growth of ZnS nanowires directly on GaAs (111)B was assisted by Au_2Ga alloyed droplets in the liquid state, which would subsequently change to a core-shell structure (Au_7Ga_2 core surrounded by Ga-rich Au_xGa_y and Ga_xO_y shells) during the cooling to room temperature and air exposure. On the other hand, the VSS growth involved a ZnS buffer layer to prevent Au-Ga interaction with the substrate and to enforce a pure solid Au catalyst. A comprehensive structural analysis was performed to study the different crystallographic phase in the NWs. The

HRTEM images analysis of VLS grown samples undoubtedly identified a 15R crystal phase, which had never been observed in ZnS nanowires. We detailed such 15R sequence and proposed selection rules to illustrate its formation. This study opens the way to a set of further characterizations such as μ-Raman and nano-cathodoluminescence to assess the optical properties of this remarkable ZnS 15R crystal structure. Regarding the NWs grown on ZnS buffer (VSS mode, solid catalyst), an HRTEM study of straight wires revealed large segments of WZ with inclusion of small ZB segments. Finally, we emphasize that ZnS is a perfect material to study polytypes in semiconductor nanowires as cohesive energy differences are small between the available crystal phases. This is a remarkable case study to understand the mechanisms and growth dynamics, which imparts the optimized conditions for crystal phase selection in such 1D nanostructures.

Acknowledgements

We acknowledge fruitful discussions with Dr. Frank Glas, C2N laboratory, France. S.K. would like to thank ED-Interfaces, Université Paris-Saclay, UVSQ for the doctoral scholarship.

Electronic Supplementary Material: Supplementary material (SEM, HRTEM images, Catalyst droplet analysis (S1), FFT of droplet, EDS measurements on catalyst droplets (S2, S3)) is available in the online version of this article

References

1] Jie, J.; Zhang, W.; Bello, I.; Lee, C.-S.; Lee, S.-T. One-dimensional ii–vi nanostructures: Synthesis, properties and optoelectronic applications. *Nano Today* **2010,** *5*, 313-336.

2] Pauzauskie, P. J.; Yang, P. Nanowire photonics. *Materials Today* **2006,** *9*, 36-45.

3] Güniat, L.; Caroff, P.; Fontcuberta i Morral, A. Vapor phase growth of semiconductor nanowires: Key developments and open questions. *Chemical Reviews* **2019,** *119*, 8958-8971.

4] Laferrière, P.; Yeung, E.; Giner, L.; Haffouz, S.; Lapointe, J.; Aers, G. C.; Poole, P. J.; Williams, R. L.; Dalacu, D. Multiplexed single-photon source based on multiple quantum dots embedded within a single nanowire. *Nano Lett.* **2020,** *20*, 3688-3693.

5] Jacobsson, D.; Panciera, F.; Tersoff, J.; Reuter, M. C.; Lehmann, S.; Hofmann, S.; Dick, K. A.; Ross, F. M. Interface dynamics and crystal phase switching in gaas nanowires. *Nature* **2016,** *531*, 317-322.

6] Glas, F.; Harmand, J.-C.; Patriarche, G. Why does wurtzite form in nanowires of iii-v zinc blende semiconductors? *Phys. Rev. Lett.* **2007,** *99*, 146101.

7] Mardix, S. Polytypism: A controlled thermodynamic phenomenon. *Phys. Rev. B* **1986,** *33*, 8677-8684.

8] Engel, G. E.; Needs, R. J. Total energy calculations on zinc sulphide polytypes. *Journal of Physics: Condensed Matter* **1990,** *2*, 367-376.

9] Ortiz, A. L.; Sánchez-Bajo, F.; Cumbrera, F. L.; Guiberteau, F. The prolific polytypism of silicon carbide. *Journal of Applied Crystallography* **2013,** *46*, 242-247.

10] Caroff, P.; Dick, K. A.; Johansson, J.; Messing, M. E.; Deppert, K.; Samuelson, L. Controlled polytypic and twin-plane superlattices in iii–v nanowires. *Nature Nanotechnology* **2009,** *4*, 50-55.

11] Hao, Y.; Meng, G.; Wang, Z. L.; Ye, C.; Zhang, L. Periodically twinned nanowires and polytypic nanobelts of zns: The role of mass diffusion in vapor−liquid−solid growth. *Nano Lett.* **2006,** *6*, 1650-1655.

12] Johansson, J.; Dick, K. A.; Caroff, P.; Messing, M. E.; Bolinsson, J.; Deppert, K.; Samuelson, L. Diameter dependence of the wurtzite−zinc blende transition in inas nanowires. *J. Phys. Chem. C* **2010,** *114*, 3837-3842.

13] Priante, G.; Harmand, J.-C.; Patriarche, G.; Glas, F. Random stacking sequences in iii-v nanowires are correlated. *Phys. Rev. B* **2014,** *89*, 241301.

14] Lopez, F. J.; Hemesath, E. R.; Lauhon, L. J. Ordered stacking fault arrays in silicon nanowires. *Nano Lett.* **2009,** *9*, 2774-2779.

15] Biswas, S.; Doherty, J.; Majumdar, D.; Ghoshal, T.; Rahme, K.; Conroy, M.; Singha, A.; Morris, M. A.; Holmes, J. D. Diameter-controlled germanium nanowires with lamellar twinning and polytypes. *Chem. Mater.* **2015,** *27*,

3408-3416.

16] Dheeraj, D. L.; Patriarche, G.; Zhou, H.; Hoang, T. B.; Moses, A. F.; Grønsberg, S.; van Helvoort, A. T. J.; Fimland, B.-O.; Weman, H. Growth and characterization of wurtzite gaas nanowires with defect-free zinc blende gaassb inserts. *Nano Lett.* **2008,** *8*, 4459-4463.

17] Jiang, Y.; Meng, X. M.; Liu, J.; Hong, Z. R.; Lee, C. S.; Lee, S. T. Zns nanowires with wurtzite polytype modulated structure. *Advanced Materials* **2003,** *15*, 1195-1198.

18] Liu, X.; Wang, D. Kinetically-induced hexagonality in chemically grown silicon nanowires. *Nano Research* **2009,** *2*, 575-582.

19] Wagner, R. S.; Ellis, W. C. Vapor - liquid - solid mechanism of single crystal growth. *Applied Physics Letters* **1964,** *4*, 89-90.

20] Dubrovskii, V. G.; Cirlin, G. E.; Soshnikov, I. P.; Tonkikh, A. A.; Sibirev, N. V.; Samsonenko, Y. B.; Ustinov, V. M. Diffusion-induced growth of gaas nanowhiskers during molecular beam epitaxy: Theory and experiment. *Phys. Rev. B* **2005,** *71*, 205325.

21] Harmand, J.-C.; Glas, F.; Patriarche, G. Growth kinetics of a single $\textinp_1\ensuremath-x\textas_x$ nanowire. *Phys. Rev. B* **2010,** *81*, 235436.

22] Fang, X.; Zhai, T.; Gautam, U. K.; Li, L.; Wu, L.; Bando, Y.; Golberg, D. Zns nanostructures: From synthesis to applications. *Progress in Materials Science* **2011,** *56*, 175-287.

23] Premkumar, S.; Nataraj, D.; Bharathi, G.; Ramya, S.; Thangadurai, T. D. Highly responsive ultraviolet sensor based on zns quantum dot solid with enhanced photocurrent. *Scientific Reports* **2019,** *9*, 18704.

24] Wang, Z.; Daemen, L. L.; Zhao, Y.; Zha, C. S.; Downs, R. T.; Wang, X.; Wang, Z. L.; Hemley, R. J. Morphology-tuned wurtzite-type zns nanobelts. *Nature Materials* **2005,** *4*, 922-927.

25] Akizuki, M. Investigation of phase transition of natural zns minerals by high resolution electron microscopy. *American Mineralogist* **1981,** *66*, 1006-1012.

26] Boutaiba, F.; Belabbes, A.; Ferhat, M.; Bechstedt, F. Polytypism in zns, znse, and znte: First-principles study. *Physical Review B* **2014,** *89*, 245308.

27] Zagorac, D.; Schön, J. C.; Zagorac, J.; Jansen, M. Theoretical investigations of novel zinc oxide polytypes and in-depth study of their electronic properties. *RSC Advances* **2015,** *5*, 25929-25935.

28] Takeuchi, S.; Suzuki, K.; Maeda, K.; Iwanaga, H. Stacking-fault energy of ii–vi compounds. *Philosophical Magazine A* **1985,** *50*, 171-178.

29] Guo, Y.; Wang, Q.; Kawazoe, Y.; Jena, P. A new silicon phase with direct band gap and novel optoelectronic properties. *Scientific Reports* **2015,** *5*, 14342.

30] Fissel, A.; Kaiser, U.; Schröter, B.; Richter, W.; Bechstedt, F. Mbe growth and properties of sic multi-quantum well structures. *Applied Surface Science* **2001,** *184*, 37-42.

31] Akopian, N.; Patriarche, G.; Liu, L.; Harmand, J. C.; Zwiller, V. Crystal phase quantum dots. *Nano Lett.* **2010,** *10*, 1198-1201.

32] Xue, M.; Li, M.; Huang, Y.; Chen, R.; Li, Y.; Wang, J.; Xing, Y.; Chen, J.; Yan, H.; Xu, H. et al. Observation and ultrafast dynamics of inter-sub-band transition in inas twinning superlattice nanowires. *Advanced Materials* **2020,** *32*, 2004120.

33] Persson, A. I.; Larsson, M. W.; Stenström, S.; Ohlsson, B. J.; Samuelson, L.; Wallenberg, L. R. Solid-phase diffusion mechanism for gaas nanowire growth. *Nature Materials* **2004,** *3*, 677-681.

34] Sue, Y.-S.; Pan, K.-Y.; Wei, D.-H. Optoelectronic and photocatalytic properties of zinc sulfide nanowires synthesized by vapor-liquid-solid process. *Applied Surface Science* **2019,** *471*, 435-444.

35] Yue, G. H.; Yan, P. X.; Yan, D.; Fan, X. Y.; Wang, M. X.; Qu, D. M.; Liu, J. Z. Hydrothermal synthesis of single-crystal zns nanowires. *Applied Physics A* **2006,** *84*, 409-412.

36] Thombare, S. V.; Marshall, A. F.; McIntyre, P. C. Size effects in vapor-solid-solid ge nanowire growth with a ni-based catalyst. *Journal of Applied Physics* **2012,** *112*, 054325.

37] Zannier, V.; Grillo, V.; Rubini, S. Diameter-dependent morphology of vapour–solid–solid grown znse nanowires. *Journal of Physics D: Applied Physics* **2014,** *47*, 394005.

38] Kodambaka, S.; Tersoff, J.; Reuter, M. C.; Ross, F. M.

Germanium nanowire growth below the eutectic temperature. *Science* **2007,** *316*, 729-732.

39] Liang, Y.; Xu, H.; Hark, S. K. Orientation and structure controllable epitaxial growth of zns nanowire arrays on gaas substrates. *J. Phys. Chem. C* **2010,** *114*, 8343-8347.

40] Geng, B. Y.; Liu, X. W.; Du, Q. B.; Wei, X. W.; Zhang, L. D. Structure and optical properties of periodically twinned zns nanowires. *Applied Physics Letters* **2006,** *88*, 163104.

41] Biswas, S.; Kar, S. Fabrication of zns nanoparticles and nanorods with cubic and hexagonal crystal structures: A simple solvothermal approach. *Nanotechnology* **2008,** *19*, 045710.

42] Rothman, A.; Forsht, T.; Danieli, Y.; Popovitz-Biro, R.; Rechav, K.; Houben, L.; Joselevich, E. Guided growth of horizontal zns nanowires on flat and faceted sapphire surfaces. *J. Phys. Chem. C* **2018,** *122*, 12413-12420.

43] Liang, Y.; Liang, H.; Xiao, X.; Hark, S. The epitaxial growth of zns nanowire arrays and their applications in uv-light detection. *J. Mater. Chem.* **2012,** *22*, 1199-1205.

44] Ramsdell, L. S. Studies on silicon carbide. *American Mineralogist* **1947,** *32*, 64-82.

45] Gibbon, D. L. Electron diffraction effects in silicon carbide. I. Pure polytypes. Ii. Whiskers. *Journal of Applied Crystallography* **1971,** *4*, 95-103.

46] Frondel, C.; Palache, C. Three new polymorphs of zinc sulfide. *Science* **1948,** *107*, 602-602.

47] Glas, F. A simple calculation of energy changes upon stacking fault formation or local crystalline phase transition in semiconductors. *Journal of Applied Physics* **2008,** *104*, 093520.

48] Zagorac, D.; Zagorac, J.; Schön, J. C.; Stojanović, N.; Matović, B. Zno/zns (hetero)structures: ıt ab initio investigations of polytypic behavior of mixed zno and zns compounds. *Acta Crystallographica Section B* **2018,** *74*, 628-642.

49] Zhdanov, G. S. The numerical symbol of close packing of spheres and its application in the theory of close packings. *Compt. Rend. Acad. Sci. URSS* **1945,** *48*, 11.

50] Johansson, J.; Bolinsson, J.; Ek, M.; Caroff, P.; Dick, K. A. Combinatorial approaches to understanding polytypism in iii–v nanowires. *ACS Nano* **2012,** *6*, 6142-6149.

51] Harmand, J.-C.; Patriarche, G.; Glas, F.; Panciera, F.; Florea, I.; Maurice, J.-L.; Travers, L.; Ollivier, Y. Atomic step flow on a nanofacet. *Phys. Rev. Lett.* **2018,** *121*, 166101.

52] Kim, Y.; Im, H. S.; Park, K.; Kim, J.; Ahn, J.-P.; Yoo, S. J.; Kim, J.-G.; Park, J. Bent polytypic znse and cdse nanowires probed by photoluminescence. *Small* **2017,** *13*, 1603695.

53] Isik Goktas, N.; Sokolovskii, A.; Dubrovskii, V. G.; LaPierre, R. R. Formation mechanism of twinning superlattices in doped gaas nanowires. *Nano Lett.* **2020,** *20*, 3344-3351.

54] Yu, H.; Wang, Q.; Yang, L.; Dai, B.; Zhu, J.; Han, J. Ultraviolet–visible light photoluminescence induced by stacking faults in 3c–sic nanowires. *Nanotechnology* **2019,** *30*, 235601.

55] Dubrovskii, V. G.; Sibirev, N. V.; Harmand, J. C.; Glas, F. Growth kinetics and crystal structure of semiconductor nanowires. *Phys. Rev. B* **2008,** *78*, 235301.

56] Panciera, F.; Baraissov, Z.; Patriarche, G.; Dubrovskii, V. G.; Glas, F.; Travers, L.; Mirsaidov, U.; Harmand, J.-C. Phase selection in self-catalyzed gaas nanowires. *Nano Lett.* **2020,** *20*, 1669-1675.

57] Johansson, J.; Zanolli, Z.; Dick, K. A. Polytype attainability in iii–v semiconductor nanowires. *Crystal Growth & Design* **2016,** *16*, 371-379.

58] Sun, Q.; Pan, D.; Li, M.; Zhao, J.; Chen, P.; Lu, W.; Zou, J. In situ tem observation of the vapor–solid–solid growth of <00̄0> inas nanowires. *Nanoscale* **2020,** *12*, 11711-11717.

59] Wen, C. Y.; Reuter, M. C.; Bruley, J.; Tersoff, J.; Kodambaka, S.; Stach, E. A.; Ross, F. M. Formation of compositionally abrupt axial heterojunctions in silicon-germanium nanowires. *Science* **2009,** *326*, 1247-1250.

60] Rueda-Fonseca, P.; Orrù, M.; Bellet-Amalric, E.; Robin, E.; Den Hertog, M.; Genuist, Y.; André, R.; Tatarenko, S.; Cibert, J. Diffusion-driven growth of nanowires by low-temperature molecular beam epitaxy. *Journal of Applied Physics* **2016,** *119*, 164303.

61] Simon, H.; Krekeler, T.; Schaan, G.; Mader, W. Metal-seeded growth mechanism of zno nanowires. *Crystal*

Growth & Design **2013,** *13*, 572-580.

62] Okamoto, H.; Massalski, T. B. The au-s (gold-sulfur) system. *Bulletin of Alloy Phase Diagrams* **1985,** *6*, 518-519.

63] Ishikawa, K.; Isonaga, T.; Wakita, S.; Suzuki, Y. Structure and electrical properties of au2s. *Solid State Ionics* **1995,** *79*, 60-66.

64] Okamoto, H.; Massalski, T. B. The au-zn (gold-zinc) system. *Bulletin of Alloy Phase Diagrams* **1989,** *10*, 59-69.

65] Cui, H.; Lü, Y. Y.; Yang, G. W.; Chen, Y. M.; Wang, C. X. Step-flow kinetics model for the vapor–solid–solid si nanowires growth. *Nano Letters* **2015,** *15*, 3640-3645.

66] Rueda-Fonseca, P.; Bellet-Amalric, E.; Vigliaturo, R.; den Hertog, M.; Genuist, Y.; André, R.; Robin, E.; Artioli, A.; Stepanov, P.; Ferrand, D. et al. Structure and morphology in diffusion-driven growth of nanowires: The case of znte. *Nano Lett.* **2014,** *14*, 1877-1883.

67] Maliakkal, C. B.; Jacobsson, D.; Tornberg, M.; Persson, A. R.; Johansson, J.; Wallenberg, R.; Dick, K. A. In situ analysis of catalyst composition during gold catalyzed gaas nanowire growth. *Nature Communications* **2019,** *10*, 4577.

68] Arbiol, J.; Kalache, B.; Cabarrocas, P. R. i.; Morante, J. R.; Morral, A. F. i. Influence of cu as a catalyst on the properties of silicon nanowires synthesized by the vapour–solid–solid mechanism. *Nanotechnology* **2007,** *18*, 305606.

69] Tuan, H.-Y.; Lee, D. C.; Hanrath, T.; Korgel, B. A. Germanium nanowire synthesis: An example of solid-phase seeded growth with nickel nanocrystals. *Chem. Mater.* **2005,** *17*, 5705-5711.

70] Dubrovskii, V. G.; Cirlin, G. E.; Sibirev, N. V.; Jabeen, F.; Harmand, J. C.; Werner, P. New mode of vapor−liquid−solid nanowire growth. *Nano Lett.* **2011,** *11*, 1247-1253.

71] Johansson, J.; Karlsson, L. S.; Dick, K. A.; Bolinsson, J.; Wacaser, B. A.; Deppert, K.; Samuelson, L. Effects of supersaturation on the crystal structure of gold seeded iii−v nanowires. *Crystal Growth & Design* **2009,** *9*, 766-773.

Electronic Supplementary Material

Induced structural modifications in ZnS nanowires via physical state of catalyst: highlights of 15R crystal phase

Sumit Kumar[1] (✉), Frédéric Fossard[2], Gaëlle Amiri[1], Jean-Michel Chauveau[1] and Vincent Sallet[1] (✉)

[1] *Groupe d'Etude de la Matière Condensée (GEMAC), Université Paris-Saclay, CNRS - Université de Versailles St Quentin en Yvelines, 45 avenue des Etats-Unis, 78035 Versailles, France*

[2] *Laboratoire d'Étude des Microstructures (LEM), CNRS-ONERA, Université Paris-Saclay, 29 avenue Division Leclerc, 92322 Chatillon, France*

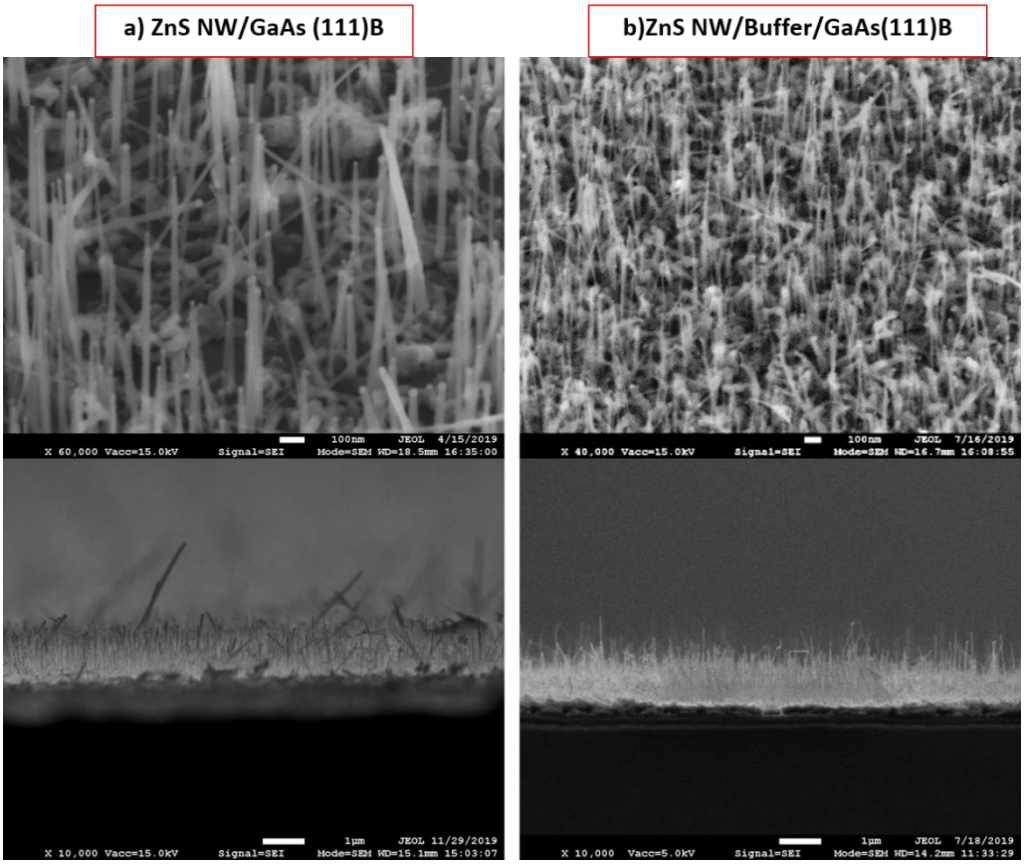

Figure S1. SEM image of nanowires grown on a) GaAs (111)B, with 90° cross-sectional view and b) Buffer/GaAs (111)B, with 90° cross-sectional view.

Address correspondence to Sumit Kumar, sumit.kumar@uvsq.fr; Vincent Sallet, vincent.sallet@uvsq.fr

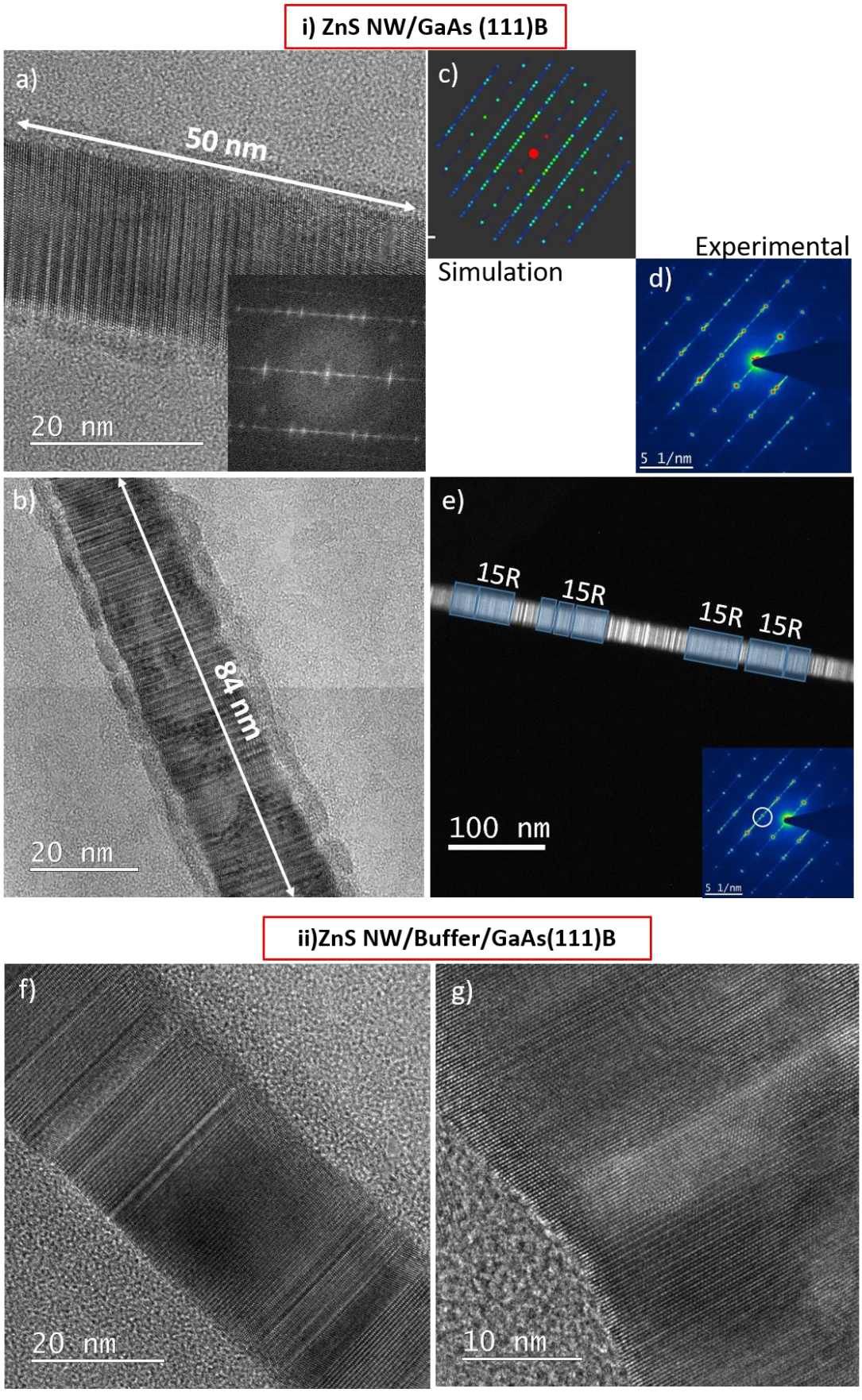
i) ZnS NW/GaAs (111)B
a)
50 nm
20 nm
c)
Simulation
Experimental
d)
5 1/nm
b)
84 nm
20 nm
e)
15R
15R
15R
15R
100 nm
5 1/nm
ii)ZnS NW/Buffer/GaAs(111)B
f)
20 nm
g)
10 nm

Figure S2. TEM analysis of catalyst-assisted ZnS nanowires : a) and b) HRTEM images of nanowires grown on GaAs (111)B, where the 15R structure is mainly preserved along the segment of the nanowire, c) Electron diffraction simulation of the 15R stacking along the <010> zone axis, d) Experimental evidence of the 15R stacking from diffraction taken along the <010> zone axis of the 15R phase, e) Dark field image taken from the same nanowire with the {104} diffraction node as evidenced in the diffraction pattern (given in the insert), the blue zones indicate the possible 15R stacking area, f) and g) Buffer/GaAs (111)B, mixed phases of zinc blende and wurtzite structure.

S-1. Transmission electron microscopy analysis. Noticeably, a drastic degradation has been observed under the electron beam for the narrowest NWs (10-15 nm), even if the voltage is reduced from 200 kV to 80 kV, so that their crystal structure could not be investigated. Figures S2-a) and b) show HRTEM images of nanowires grown on GaAs (111)B, without buffer, where the 15R structure is mainly preserved along the segment, with a few tens of nanometers length. HRTEM provides a direct evidence of the 15R phase (see figure 3 of the manuscript) but it is very limited in terms of the investigated area (few tens of nm). To increase the area of investigation, we have performed conventional TEM (bright field and dark field) and diffractions on several tens of nanowires from the 'VLS' sample. Figure S2-c) is the simulated diffraction pattern from the 15R structure. The signature of the 15R phase is given in diffraction by this peculiar pattern (*i.e.* a 5th order superstructure) along this zone axis. Such 15R diffraction pattern has been observed in all investigated wires, with a diameter dispersion from 15 to 40 nm. We have no evidence that a critical diameter prevents or inhibits the 15R growth with respect to this investigated range of nanowire diameters. To evidence the 15R stacking along the nanowire, we have taken dark field images using the {104} diffraction vector, a diffraction condition sensitive to the 15R phase. The figures S2-e) displays a dark field image of a representative NW and it shows that the polytype formation is not observed all along the nanowire but only on certain segments indicated by the blue zones.

S-2. Catalyst droplet analysis. In the first case (*i.e.* NW grown on GaAs (111)B, Figure S3a), HRTEM image taken from [001] axis, the catalyst is similar to a spherical droplet in the shape. In the literature, different phases (Au_7Ga_2, Au_2Ga, AuGa) of the Au-Ga alloyed catalyst have been reported [1–3]. The FFT pattern of the HRTEM image corresponds to the Au_7Ga_2 phase of the catalyst at room temperature. However, all the catalyst droplets studied in this sample do not present such a clear signature and are related to neither Au_7Ga_2 nor Au_2Ga, indicating a heterogeneity of the Au-Ga solid phase. More information will be given in the EDS section.

In the second case (*i.e.* NW grown on buffer layer, Figure S3b), the catalyst shows a facetted shape and the FFT pattern confirms the pure gold phase of the catalyst with a face-centered cubic structure. Interplanar distances were calculated as 0.239 nm and 0.206 nm which corresponds to (111) and (002) planes respectively. The [002] axis of the gold catalyst is parallel with the [0001] or the [111] axis of the NW. Moreover, the facets present on the droplet are (111) oriented and compatible with solid gold particles [4]. This occurrence suggests the VSS growth process of the NWs. Surprisingly, in all TEM images (around 20 NWs), we noticed a 2.9 nm thick shell formed around the catalyst for the NW directly grown on GaAs (111)B while no shell was developed for NW grown with ZnS buffer layer.

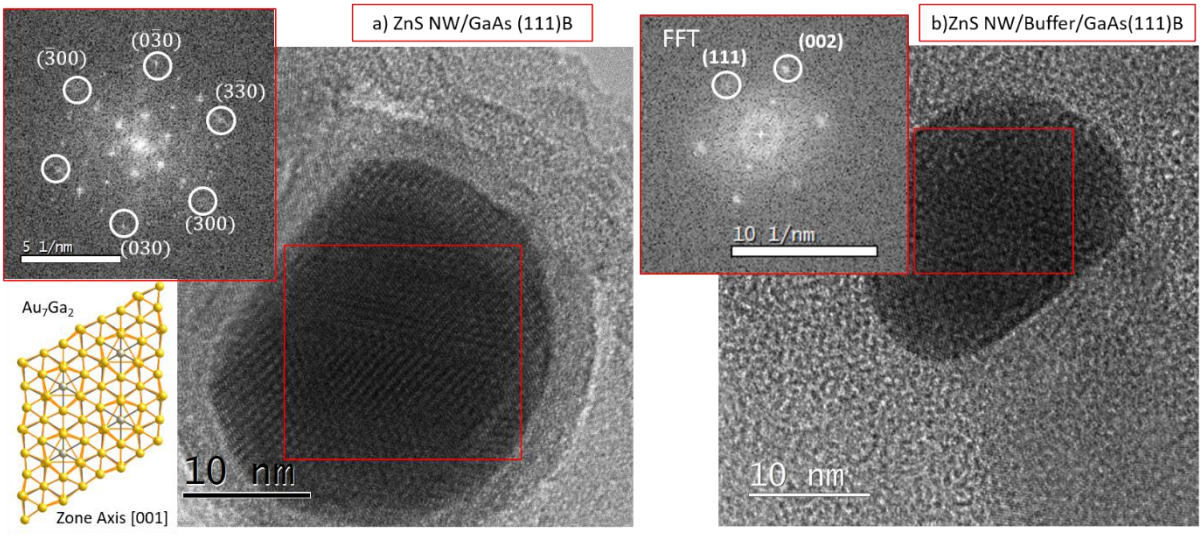

Figure S3. HRTEM image of the catalyst present at the top of a ZnS nanowire grown on a) GaAs (111)B, the FFT pattern of the HRTEM image taken in [001] zone axis reveals Au_7Ga_2 phase of the catalyst, and b) ZnS buffer/GaAs (111)B, a faceted catalyst droplet can be seen in the HRTEM image and the corresponding cubic phase from the FFT pattern emphasizes the pure Au solid phase of the droplet.

S-3. EDS of catalyst droplet. EDS analysis of the catalyst droplet present at the top of the nanowire was performed. EDS mappings are illustrated in the Figure S4. Regarding NWs grown directly on GaAs (111)B, Ga and Au contents are detected (Figure S4b-c), but no presence of Zn or S (or below the detection limit) has been found. At first sight, the area of Ga mapping appears to be larger than the one of Au, indicating that Au is more distributed at the center. It matches with the HAADF image (Figure S4d) which manifests that the droplet is surrounded by two shells, possibly a Ga-rich shell and a GaO shell, respectively. This core/shell structure could be induced during the cooling. Additionally, the compositional measurements were carried out on four different catalyst droplets, and were found to be non-homogeneous, as already mentioned above. An Au-rich phase from 61 to 78% Au and 22 to 39% Ga (see detailed measurements in section S-4) has been perceived. We suggest that the catalyst droplet is liquid after the dewetting on GaAs (111)B and would exhibit an Au_2Ga phase (33% Ga, corresponding to the eutectic composition), and that the growth of the NWs takes place *via* this liquid Au_2Ga alloy [5, 6]. Subsequently, during the cooling, the Ga diffuses from the core toward the surface, leaving an Au_7Ga_2 (as observed in Figure S3a) or at least an Au-rich core, and oxidizes on the surface to form a GaO shell. On the other hand, EDS analysis of the tip of a nanowire grown with ZnS buffer only shows the presence of gold with no detectable traces of gallium, Zn, or S, in agreement with FFT pattern observations.

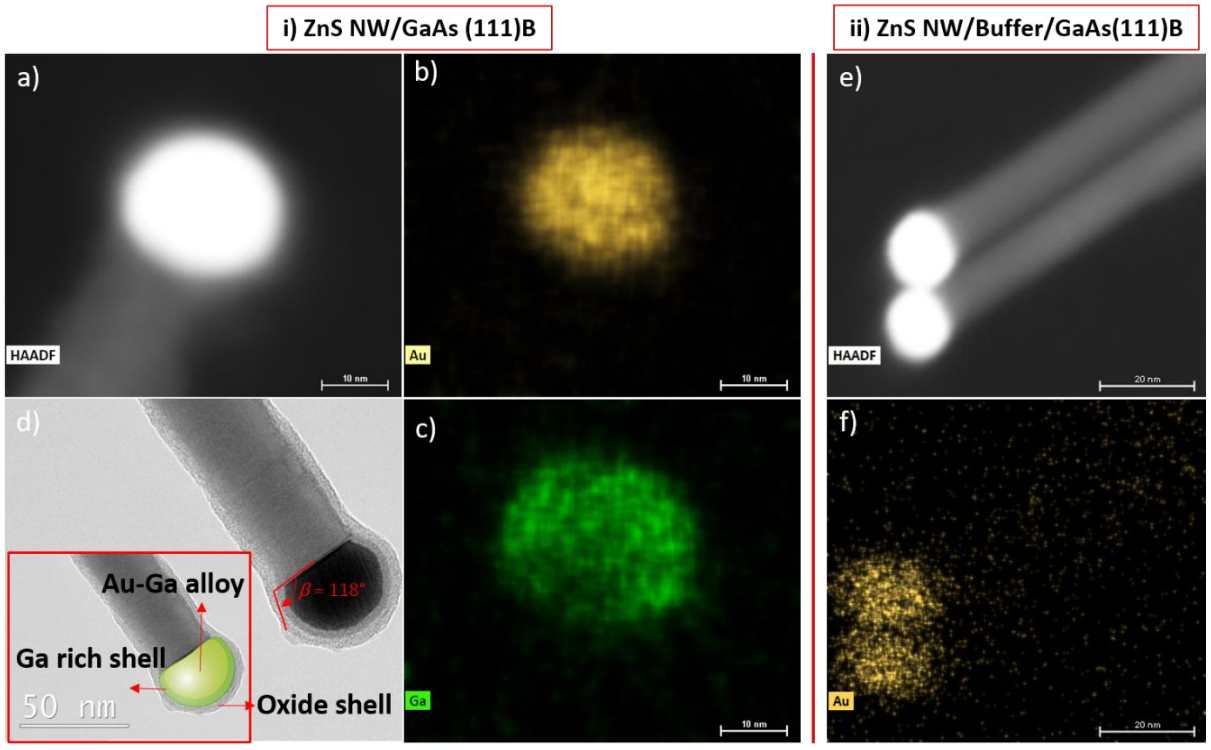

Figure S4. a) HAADF image of the catalyst present at the top of VLS grown nanowire, b) EDS gold mapping of VLS ZnS NWs, c) EDS gallium mapping of VLS ZnS NWs, d) Ga-rich shell and oxide shell surrounding the Au-Ga catalyst droplet, e) HAADF image of the catalyst for VSS grown nanowire, f) EDS gold mapping of VSS ZnS NWs.

S-4. EDS measurements of catalyst droplets. In this section, the EDS measurements were focused on the catalyst droplet present at the top of VLS grown ZnS NWs. Measurements were performed on the four different catalyst droplets and carried out on the whole ensemble of catalyst droplet as well as focus on the core of the droplet as shown in the Figure S5. These measurements were done to study the spread of the Gallium inside the droplet. The compositional values of gold and gallium are summarized in Table S1. The compositional values of Au and Ga were found to be non-homogenous, as the core of the droplet found to be richer in Au compared to the whole ensemble. A low composition of Ga in the core compared to the whole ensemble suggests that the Ga diffuses towards the surface of the catalyst droplet to get oxidized to form a GaO shell.

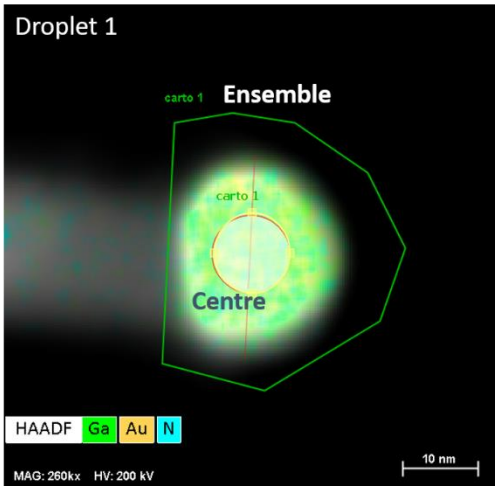

Figure S5. EDS measurements were performed on ensemble and at the core (center) of catalyst droplet for VLS grown ZnS NWs. The gallium and gold composition are found to be 10.6 and 89.3 % at centre, and 22 and 78 % in the ensemble.

Droplet	Measurements	Gallium (%)	Gold (%)
1.	Center	10.6	89.3
	Ensemble	22.0	78.0
2.	Center	23.7	76.3
	Ensemble	35.8	64.1
3.	Center	22.8	77.2
	Ensemble	38.7	61.3
4.	Center	28.6	71.4
	Ensemble	38.4	61.6

Table S1. The compositional values of gold and gallium measured for the different catalyst droplets at their center and for the whole ensemble of droplet. The measurements were carried on four different catalyst droplets.

References

[1] Harmand, J. C.; Patriarche, G.; Péré-Laperne, N.; Mérat-Combes, M.-N.; Travers, L.; Glas, F. Analysis of Vapor-Liquid-Solid Mechanism in Au-Assisted GaAs Nanowire Growth. *Applied Physics Letters*, **2005**, *87*, 203101.

[2] Zannier, V.; Grillo, V.; Martelli, F.; Plaisier, J. R.; Lausi, A.; Rubini, S. Tuning the Growth Mode of Nanowires via the Interaction among Seeds, Substrates and Beam Fluxes. *Nanoscale*, **2014**, *6*, 8392–8399.

[3] Wang, Z.; Wang, Y.; Zhou, X.; Yang, Z.; Yin, Y.; Zhang, J.; Han, N.; Ho, J. C.; Chen, Y. Controlled Growth of Heterostructured Ga/GaAs Nanowires with Sharp Schottky Barrier. *Crystal Growth & Design*, **2018**, *18*, 4438–4444.

[4] Bellet-Amalric, E.; Elouneg-Jamroz, M.; Rueda-Fonseca, P.; Bounouar, S.; Hertog, M. D.; Bougerol, C.; André, R.; Genuist, Y.; Poizat, J. P.; Kheng, K.; et al. Growth of II–VI ZnSe/CdSe Nanowires for Quantum Dot Luminescence. *Journal of Crystal Growth*, **2013**, *378*, 233–237.

[5] Wang, Y.; Yang, Z.; Wu, X.; Han, N.; Liu, H.; Wang, S.; Li, J.; Tse, W.; Yip, S.; Chen, Y.; et al. Growth and Photovoltaic Properties of High-Quality GaAs Nanowires Prepared by the Two-Source CVD Method. *Nanoscale Research Letters*, **2016**, *11*, 191.

[6] Han, N.; Wang, Y.; Yang, Z.; Yip, S.; Wang, Z.; Li, D.; Hung, T. F.; Wang, F.; Chen, Y.; Ho, J. C. Controllable III–V Nanowire Growth via Catalyst Epitaxy. *J. Mater. Chem. C*, **2017**, *5*, 4393–4399.